Cold Regions Science and Technology 121 (2016) 167–178

Contents lists available at ScienceDirect

Cold Regions Science and Technology

journal homepage: www.elsevier.com/locate/coldregions

Inferring the variation of climatic and glaciological contributions to West Greenland iceberg discharge in the twentieth century

Yifan Zhao [c], Grant R. Bigg [b,*], Steve A. Billings [a], Edward Hanna [b], Andrew J. Sole [b], Hua-liang Wei [a], Visakan Kadirkamanathan [a], David J. Wilton [b]

[a] Department of Automatic Control and Systems Engineering, University of Sheffield, Sheffield S10 2TN, UK
[b] Department of Geography, University of Sheffield, Sheffield, S10 2TN, UK
[c] School of Aerospace, Transport and Manufacturing, Cranfield University, Cranfield, MK43 0AL, UK

ARTICLE INFO

Article history:
Received 17 January 2014
Received in revised form 30 July 2015
Accepted 1 August 2015
Available online 17 August 2015

Keywords:
Greenland
Iceberg
Ice sheet
Ocean temperature
Climate
Systems modelling

ABSTRACT

Iceberg discharge is a major component of the mass balance of the Greenland Ice Sheet (GrIS). While bulk estimates of discharge variation over time exist, inferred remotely from measurements of grounding line ice velocities or surface mass balance calculations, few detailed measurements of discharge itself from individual marine-terminating glaciers existed until recent years. Recently, it has been shown, through a combination of ocean–iceberg modelling and non-linear system identification, that the century-long record of iceberg numbers crossing 48°N in the West Atlantic is a good first-order proxy for discharge from at least south and west Greenland. Here, we explore the varying relative importance of ice sheet, oceanic and climatic forcing of iceberg discharge from these areas over the twentieth century, by carrying out sensitivity studies of a non-linear auto-regressive mathematical model of the 48°N time series. We find that the relationships are mainly non-linear, with the contribution of the GrIS surface mass balance to iceberg discharge likely to be dominant in the first half of the century. This period is followed by several decades where oceanic temperature effects are most important in determining the model variation in iceberg discharge. In recent decades, all physical processes play a non-negligible part in explaining the iceberg discharge and the model suggests that the glacial response time to environmental changes may have decreased.

1. Introduction

The total mass balance of the Greenland Ice Sheet (GrIS) comes from the net mass balance between surface accumulation/runoff, basal melting, and ice discharge through calving. The former is known as the surface mass balance (*SMB*)—the balance between net precipitation and surface ablation (surface meltwater, runoff, and sublimation)—and has been calculated by a number of groups using different atmospheric reanalysis and/or regional climate model fields as forcing for various melt/runoff/*SMB* models (e.g. Hanna et al., 2011; Janssens and Huybrechts, 2000; van den Broeke et al., 2009). While there are differences between these *SMB* models, they are second order in magnitude, and all show a distinct trend towards a reduced *SMB* over the last decade (e.g. Box, 2013; Fettweis et al., 2008; Hanna et al., 2011; Van den Broeke et al., 2009), but with considerable interannual variability (e.g. Fig. 1). This recent trend is part of a longer-term *SMB* decrease, starting around 1930 (Hanna et al., 2011). But what characterises this record throughout, both recently and over the last century or more, is high variability on an annual timescale. The ice discharge term (D) in the total mass balance, although estimated to have earlier contributed approximately equally to ice sheet mass loss as the *SMB* (Rignot et al., 2011) but more recently only a third of the latter's magnitude (Enderlin et al., 2014), has not been directly measured, but estimated empirically (e.g. Bigg, 1999; Reeh, 1994) or, more recently, inferred from a combination of satellite remote sensing of ice motion across the ice sheet's grounding line and ice thickness (e.g. Enderlin et al., 2014; Rignot et al., 2008, 2011; Sasgen et al., 2012; van den Broeke et al., 2009). While D inferred from grounding line discharges has shown a distinct upward trend in the last decade, in contrast to the *SMB* time series it is characterised by a lack of interannual variability.

However, what measures we do have for annual variations in iceberg discharge suggest that D—when taken as the calving flux from the GrIS, rather than transport over the grounding line—is actually highly variable. At the individual glacier scale, it is well known that the major glacier of west Greenland—Jacobshavn Isbrae—has long exhibited substantial changes in discharge from year to year and decade to decade (e.g. Csatho et al., 2008; Sohn et al., 1998). Similarly, there has been short-term major ice loss from northwest Greenland glaciers on different occasions in the last few decades (Kjaer et al., 2012). The International

* Corresponding author. Tel.: +44 1142227905.
E-mail address: grant.bigg@sheffield.ac.uk (G.R. Bigg).

http://dx.doi.org/10.1016/j.coldregions.2015.08.006

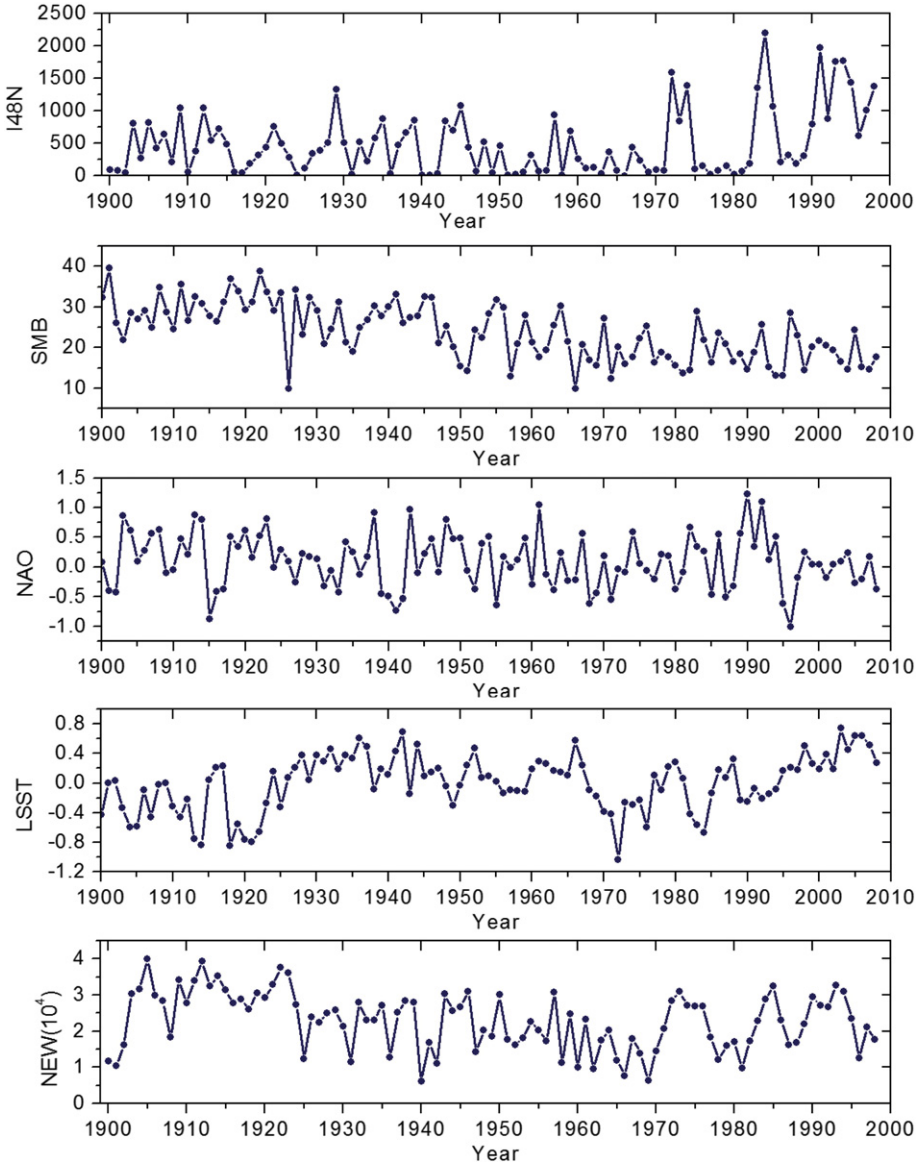

Fig. 1. The annual input and output variables for the Greenland Iceberg Calving modelling problem. Units are number (I48N), $\times 10$ km^{3}yr^{-1} water equivalent (*SMB*), standardised value (*NAO*), °C anomaly (*LSST*), $\times$10,000 km^2 (*NEW*; 1900–1998 only).

Ice Patrol's (IIP) long-term record of icebergs crossing 48°N (I48N; Marko et al., 1994; Murphy and Cass, 2012), an integrated measure of iceberg flux from at least south and west Greenland (Bigg and Wilton, 2014), and one which is highly variable on an annual scale (Fig. 1), has been shown to be a first-order proxy for west Greenland iceberg discharge (Bigg et al., 2014), down to individual glacier level (Wilton et al., 2015).

The mechanisms which control glacier retreat, and therefore calving, have recently been discussed in a review article by Straneo et al. (2013). Here three categories of triggering mechanisms for retreat are presented. The first is submarine melting at the ice–ocean interface, linked to changes in ocean temperature (Seale et al., 2011) and variation in ice sheet runoff (Motyka et al., 2013; Slater et al., 2015), which can alter the ice front force balance. The second is variation in the thickness, extent, and duration of the calved ice/sea-ice melange in front of marine-terminating glaciers. This melange has been shown to hinder calving over winter and into the spring (Todd and Christoffersen, 2014; Walter et al., 2012) and is likely to be linked to a combination of glaciological and ocean and atmosphere temperature and circulation change (Mugford and Dowdeswell, 2010). The third is the nature of crevassing and sub-glacial hydrology close to the glacier's calving front. This factor will be linked to changes in surface melting and runoff via the amount and depth of water-filled crevasses and routing of runoff at the base of the glacier (e.g. Andersen et al., 2011; Moon et al., 2014).

Previously we have used a combination of ocean–iceberg modelling and the non-linear system modelling discussed below to examine these mechanisms at annual timescale (Bigg et al., 2014). In this paper, we examine in much greater detail the variation and sensitivity of these mechanisms over time by using non-linear finite impulse response (NFIR) system identification modelling of the discharge signal in I48N. The NFIR approach is described below in the Methods section, but, briefly, it is a modelling framework, derived from control engineering, which allows the user to construct linear or non-linear dynamic models between inputs (exogenous variables) and outputs (auto-regressive variables) in the presence of coloured and non-linear noise. Three physical variables that we use as model inputs to characterise the large-scale physical environment in which the Greenland marine-terminating outlet glaciers exist are the *SMB*, representing the glacier's surface runoff/accumulation balance, a measure of regional ocean temperature (the Labrador Sea Surface Temperature; *LSST*), which, indirectly

through winter mixing in the Labrador Sea, affects submarine-ice melting, and an atmospheric circulation measure (North Atlantic Oscillation, *NAO*). The latter has been shown to be linked to Greenland coastal temperatures (Hanna et al., 2013). In addition, it has previously been shown by Marko et al. (1994) that there is a significant correlation between a measure of winter sea-ice off Newfoundland (NEW; Hill and Jones, 1990) and I48N. This variable is also included as a model input, although, unlike the other three inputs, it is difficult to see how a measure of west Labrador Sea sea-ice could be a causal factor in the calving of icebergs. In all cases, we have chosen large-scale quantities for our model inputs as we seek to model mean calving behaviour over extensive areas of Greenland, rather than in individual fjords.

2. Method

2.1. Data

As discussed in the Introduction, the input variables to be used in developing NFIR models of I48N were chosen to be surface mass balance (*SMB*), North Atlantic Oscillation (*NAO*), the Labrador Sea Surface Temperature (*LSST*), and the sea-ice in the Newfoundland area (*NEW*). The output variable that we attempt to model is I48N (Fig. 1), the monthly iceberg count from the U.S. Coast Guard's IIP over 1900–2008 (see http://www.navcen.uscg.gov/pdf/iip/International_Ice_Patrols_Iceberg_Counts_1900_to_2011.pdf). This includes all separate icebergs, of whatever origin, greater than 5 m in above-water length observed south of a line extending along 48°N from the Newfoundland coast to approximately 40°W. A full discussion of this time series is contained in a range of past literature (Berkson et al., 2010; Christensen and Luzader, 2012; Marko et al., 1994; Murphy and Cass, 2012), with some verification of its detail compared to a shorter record of individual icebergs in the Labrador Sea by Wilton et al. (2015). While the construction of the time series has not been homogeneous over time, as the detection methods have changed radically from ships to radar, satellite, and modelling (Christensen and Luzader, 2012), it has always been the purpose of the IIP to prevent a major incident like the sinking of the MS *Titanic* in the busy shipping routes into eastern North America (Murphy and Cass, 2012). The lack of serious iceberg-related incidents in the area since 1913 (Murphy and Cass, 2012) is consistent with I48N being a reliable time series, as is the lack of discontinuities in the series when observation systems changed. The likelihood of greater error during the earlier period needs to be borne in mind, however.

The input variables come from a variety of sources. Three come from existing work. The monthly *NAO* time series comes from Hurrell and Deser (2009) and is the principal component-based version of this atmospheric circulation index (Fig. 1). The Greenland *SMB* originates from Hanna et al. (2011). It is based on a positive degree day runoff/retention model (Janssens and Huybrechts, 2000), with the *SMB* series (Fig. 1) being a composite based on twentieth century reanalysis (1871–1957; Compo et al. 2011) and ECMWF (ERA40 reanalysis 1958–2001, plus ECMWF operational analysis 2002–2010) temperature, and precipitation datasets that were calibrated/validated against in situ data and spliced together. Hanna et al. (2011) demonstrates that this splicing led to little modification in the series constructed purely from the twentieth century reanalysis. The NEW series (Fig. 1) is an extension, until 1998, of the January–April mean sea-ice area south of 56°N presented by Hill and Jones (1990). The one input variable generated for this paper is *LSST* (Fig. 1). This comes from averaging the Kaplan v2 SST (Kaplan et al., 1998), over the Labrador Sea area east to 45°W, and south from the Davis Strait to 55°N. While this is on the edge of the area covered by the Kaplan et al. global analysis, their error analyses suggest that the field in this region is not especially dependent on differences in the analysis method, and errors do not vary substantially over the twentieth century.

The raw datasets of I48N, *SMB*, *NAO*, and *LSST* consist of 1308 monthly data points starting from the January of 1900 and extending to the December of 2008. The analysis reported below was initially conducted with yearly averages calculated from the monthly time series of I48N, and averaging the values of *SMB*, *NAO*, and *LSST*, within 12 calendar months. Only annual data are available for NEW, covering 1900–1998, which is why this initial approach used calendar years rather than the October–September period used to define an iceberg year by the IIP. The anual data for each variable will be denoted as

$$I48N_a(k), SMB_a(k), NAO_a(k), LSST_a(k), NEW_a(k), k = 1900, 1901, \ldots, 1998$$

and the monthly data are expressed as$I48N_m(k)$, $SMB_m(k)$, $NAO_m(k)$, $LSST_m(k)$, $k = 1, 2, \ldots, 1308$.

Fig. 1 shows the annual raw data from 1900 to 1998 for the four inputs and I48N.

2.2. The NFIR model

In this study, a non-linear finite impulse response (NFIR) model, also known as a Volterra Non-linear Regressive with Exogenous Inputs model, expressed as

$$y(k) = f\left(u_1^{[k-1]}, u_2^{[k-1]}, \ldots, u_r^{[k-1]}\right) + \varepsilon(k) \tag{1}$$

was considered to represent a multi-input and single-output system, where $k(k = 1, 2, \ldots)$ is a time index, r is the number of the system inputs, f is some unknown linear or non-linear mapping which links the system output $y(k)$ to the system inputs $u_1(k)$, $u_2(k)$,..., $u_r(k)$; $\varepsilon(k)$ denotes the model residual. The symbol $u_i^{[k-1]}(i = 1, 2,..., r)$ is defined as:

$$u_i^{[k-1]} = [u_i(k), u_i(k-1), u_i(k-2), \ldots, u_i(k-n_i)] \tag{2}$$

where n_i is the maximum temporal lag to be considered for the system input u_i. The NFIR model is a special case of the Nonlinear Auto-Regressive Moving Average with eXogeneous inputs (NARMAX) model (Leontaritis and Billings, 1985a, 1985b). The general form of the NARMAX model can be expressed as

$$y(k) = f\left(y^{[k-1]}, u_1^{[k-1]}, u_2^{[k-1]}, \ldots, u_r^{[k-1]}, \varepsilon^{[k-1]}\right) + \varepsilon(k) \tag{3}$$

where the regressions of the output $y^{[k-1]}$ and the noise $\varepsilon^{[k-1]}$ are included. The NFIR model only considers a single noise term $\varepsilon(k)$ that can often be treated as an independent, identically distributed zero mean noise sequence. In this study, a full NARMAX model has been tested and insignificant improvement in model performance was achieved comparing with the NFIR model. This means that auto-regressive behaviour is significant, and for simplicity, only the NFIR model will therefore be considered in this paper.

A commonly employed model type is to specify the function f in (1) as a basic function expansion using a linear parameters form (Chen and Billings, 1989; Wei et al., 2004), which can be expressed as

$$y(k) = \sum_{m=1}^{N} \theta_m \Phi_m(k) + \varepsilon(k) \tag{4}$$

where $\Phi_m(k)$ are the m th model terms generated from all the regressor vectors, θ_m are unknown parameters, and N is the total number of potential model terms. Note that $\Phi_m(k)$ are, in general, non-linear polynomials.

2.3. Model term selection

A number of effective algorithms exist that can automatically select the correct model structure and hence can determine, from the data only, whether the most appropriate model is linear or non-linear. The methods therefore automatically determine the simplest model that is

appropriate for representing the dataset that is analysed (Billings, 2013; Billings and Wei, 2007; Chen et al., 1989; Wei et al., 2009). In this paper, a routine called adaptive–forward–OLS, shown in the Appendix A, was employed to determine the model structure and estimate the unknown parameters.

2.4. Tracking variables, lags, linearity and non-linearity

The value of the error reduction ratio (ERR) for each selected term describes the percentage this term contributes to the output. This section aims to extract the contribution of each input variable, and the contribution of a specific regression with a certain time lag for an input.

The sum of ERR values of all selected terms is defined as

$$SERR = \sum_{i=1}^{N} [err]_i \tag{5}$$

to describe the percentage explained by the identified model to the system output, where N denotes the number of the selected terms. The contribution of the i th input variable to the variation of the system output, denoted as $ERRC_{u_i}$, is defined as the sum of ERR values of the terms that include this input variable. Because some selected terms may involve more than one input variable, the sum of $ERRC_{u_i}$ for all input variables can be greater than $SERR$. To aid interpretation, $ERRC_{u_i}$ is normalised and written as

$$ERRC_{u_i} = \frac{\sum_{j=1}^{N}\left([err]_j : u_i \in \Phi_j\right)}{\sum_{p=1}^{r}\sum_{j=1}^{N}\left([err]_j : u_p \in \Phi_j\right)} \times SERR \tag{6}$$

The contribution of the regression $u_i(k-l)$ at the time lag l for the i th input variable is given as

$$ERRC_{u_i(k-l)} = \frac{\sum_{j=1}^{N}\left([err]_j : u_{i(k-l)} \in \Phi_j\right)}{\sum_{p=1}^{r}\sum_{j=1}^{N}\left([err]_j : u_p \in \Phi_j\right)} \times SERR \tag{7}$$

The linear contribution from inputs can be expressed as the sum of the ERR value of the linear terms, and the quadratic contribution can be expressed as the sum of the ERR value of the quadratic terms, and so on.

A window, within which the model is assumed stationary, is used to identify the NFIR model, and then the model terms and corresponding ERR contribution are tracked by sliding the window through the data step by step. The required window size of sampled data depends on the dynamical properties of the original signals and the complexity of the chosen model structure. A selection of small window size means a fast reaction to the change of contribution over time, but it may lead to insufficient data to achieve an accurate result. Conversely, a selection of a large window size can improve the accuracy of contribution, but it may significantly slow down the modelled reaction to the change of contribution over time. Many sensitivity experiments were carried out, with the conclusion being that a window size of 30 years, a choice dependent on the dominant frequency of the evolving signals, was appropriate.

Traditional methods to track time variation systems, such as recursive least squares, least mean squares, or a Kalman filter etc., use a fixed model structure to describe the system and track the changing of parameters. Alternative approaches have been reported by Zou and Chon (e.g. Zou and Chon, 2004; Zou et al., 2003). The approach described here, an extension of the causality detection method recently developed for a medical application (Zhao et al., 2012), is totally novel because it tracks the model structure and so allows us to follow the evolution of the contribution of variables, lags, and the nature of the model terms, which is not possible to achieve using other methods. This approach, therefore, is a fundamentally new way of modelling time variation in systems. Here, we will use this method on the I48N time series to reveal important insights into mass balance change over western Greenland and to investigate how the influence of different physical effects vary over time. It needs to be remembered, however, that there are likely to be factors not included here which influence I48N and that errors in the various datasets are likely to decrease with time, so we do not expect to account for all the variance in I48N in the models presented here.

3. Results

A set of sensitivity studies of the I48N NFIR model structure was developed for both annual and monthly datasets. For each temporal resolution, a model using all input variables is shown and described. We then successively remove terms to understand the model dependence on the number of input variables. This also helps confirm the robustness of the full model, as we would expect the basic importance of a particular variable to be consistent in each sensitivity test in which it was used. We start, however, by seeking the maximum time lag terms to be included in our modelling by evaluating the cross-correlation coefficients of I48N with each of our environmental variables.

3.1. Test1: Annual data analysis

Based on (2), the complexity of the NFIR model depends on the maximum time lag n_i. Assuming the number of inputs is r and the maximum time lag for each input is n, then, considering linear terms only, the number of possible candidate terms is

$$(n+1) \times r + 1.$$

If also considering quadratic terms, the number of possible candidate terms is

$$\frac{((n+1) \times r + 1)((n+1) \times r + 2)}{2},$$

and if the model also considers cubic terms, the number of possible candidate terms becomes

$$\frac{((n+1) \times r + 1)((n+1) \times r + 2)((n+1) \times r + 3)}{6}.$$

To determine the appropriate maximum time lag for the NFIR model, the cross-correlation coefficients between I48N and each input were calculated (Fig. 2). From these results, the maximum significant time lag was observed at −3 years, in the cross-correlation between the I48N and *LSST*. Hence, the maximum time lag for the annual NFIR models used in this paper was chosen to be 1 year greater than this to ensure all terms of significance were captured by the model. For the below NFIR model fitting, the linear, quadratic, and cubic terms were all considered.

3.1.1. Full variables modelling using sliding windows

The full annual NFIR model uses a sliding window with a width of 30 years to track the contribution of each, and every, input variable (*LSST*, *NAO*, *NEW*, and *SMB*) over time. Fig. 3 shows the comparison of the annual I48N and the model's output, where the output at the year t was calculated by the model obtained from the window $[t-15, t+14]$. The impact of the sliding window on the temporally varying contribution of each input variable, computed by (6), is shown in Fig. 4. Terms involving *NEW* provide the largest ERR signal for ~90% of the century, but from the late 1930s through to the 1970s, the terms involving *SMB* are mostly of a similar magnitude, with both contributing ~40% of

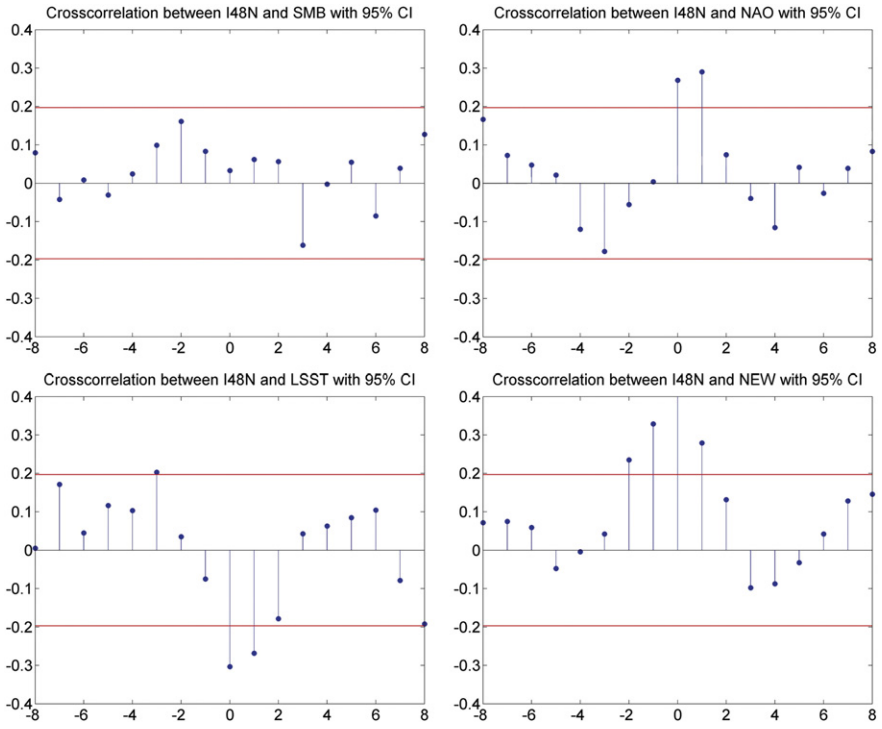

Fig. 2. Cross-correlation coefficients between annual time series of I48N and each input variable, with corresponding 95% confidence levels. These are shown by lines near ±0.2; coefficients with lags out to ±8 years are shown.

the signal. It is noteworthy that in the 1970s, *LSST* is the largest contributor to the model, with its contribution to the I48N signal exceeding 40%. Terms involving *NAO* are always of secondary importance. A linear term is dominant in the sliding model window only between 1920 and 1935 (Fig. 5); for the remaining 50 years, cubic behaviour is the overwhelmingly dominant term in the model.

The sliding window model has shown a complex, and evolving, relationship between I48N and the four input variables over the twentieth century. It shows times when different physical factors underlying our input variables are statistically more or less important in determining the mean iceberg discharge from the western half of Greenland. We will investigate this difference in more detail in the following sections, but first it is of note that the terms involving *NEW* are usually without a time lag. As has been recognised in the past (Marko et al., 1994), there is a strong correlation between I48N and the local sea-ice conditions in the winter immediately preceding the peak iceberg season of mid-late spring. However, the local sea-ice conditions off Newfoundland cannot physically determine the GrIS calving flux, which essentially derives from the previous year's summer calving (Howat et al., 2010), or even earlier years (Bigg and Wilton, 2014). The calving leading to the I48N flux will have already occurred before the late winter sea-ice conditions described by the variable *NEW* (Hill and Jones, 1990). The strong correlation must therefore be due to a mutual response to some oceanic and/or atmospheric forcing extending over the previous 6 months to a year, and likely to be related to the probability of icebergs being trapped within coastal sea-ice pack. This has recently been shown to be the most likely reason for the timing of the spring/early summer I48N (Wilton et al., 2015). In the remainder of the sensitivity studies discussed here, we therefore exclude *NEW* from our list of input variables.

3.1.2. Three input variables: SMB, NAO, and LSST

In this test, there were three inputs (*SMB*, *NAO*, and *LSST*). Note that the length of our annual inputs datasets has lengthened, to 1900–2008, by excluding *NEW*. The NFIR model for this case can be written as

$$\begin{aligned} I48N_a(k) = \; & f(SMB_a(k), SMB_a(k-1), \ldots, SMB_a(k-4), \\ & NAO_a(k), NAO_a(k-1), \ldots, NAO_a(k-4), \\ & LSST_a(k), LSST_a(k-1), \ldots, LSST_a(k-4)) \\ & +\varepsilon(k) \end{aligned} \tag{9}$$

A sliding window of length 30 years was used to track the temporal variation of the model, and so the contribution of each input variable. With the removal of *NEW*, terms involving *SMB* provide half of the ERR signal, or more, for much of the century (Fig. 6a), although *LSST* contributes a similar proportion to ERR during the 1960s and '70s, as before. Note that during the 1980s and '90s, all inputs provide at least a contribution of 15% to ERR in the model, before *SMB* returns to dominance in recent years. It is noteworthy that the sum of ERR for the

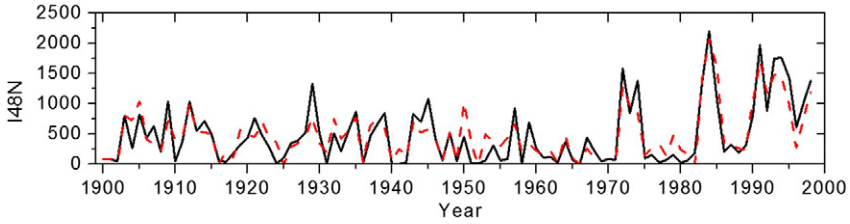

Fig. 3. A comparison of I48N (solid) with the model output of the NFIR model based on temporal sliding windows of 30 years (dashed). Four input variables (*SMB*, *NAO*, *LSST*, and *NEW*) were considered.

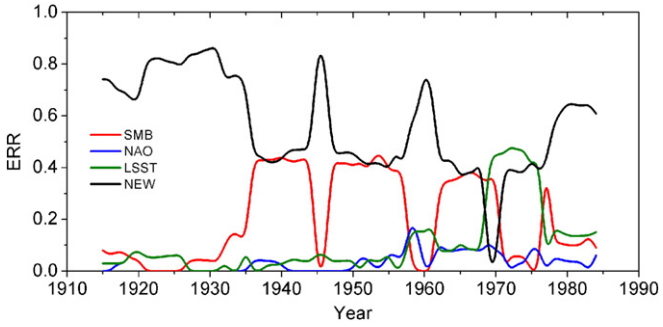

Fig. 4. Computed contributions of the four input variables to I48N over 1900–1998, based on the ERR values for a 30-year sliding window which is incremented 1 year at a time. To avoid inconsistencies in presentation due to initial and final conditions in the dataset, the initial (before 1915) and final (after 1984) ERR contributions were ignored due to insufficient samples.

three input variables is very similar (80–90%) to that from using *NEW* as well, consistent with our argument that the latter is not a fundamental forcing variable in the system, but merely responding to a common forcing of I48N.

When *SMB* tends to be dominant in the first half of the twentieth century, the leading model term, explaining 60% of ERR, is linear (Fig. 7), but during periods of more complex interactions between the model terms, during the 1950s–1990s, a cubic polynomial is most important, providing up to 90% of the ERR signal. We also examine how the temporal lags of the terms in the sliding Eq. (9) change in Fig. 8. While the variation of lag over time is complex, 40–50% of the ERR is explained by zero lag *SMB* terms for much of the first half of the century and 1-year lag more recently. Nevertheless, there are some periods in the first half of the century when the 2-year lag term also contributes similar levels to ERR. These lag times correspond well to the range of modelled travel times of icebergs from most of the west Greenland coast to 48°N (Bigg and Wilton, 2014; Wilton et al., 2015), with zero lag linked to discharge from southern Greenland and 1- and 2-year lags linked to discharge from closer and further reaches of Baffin Bay, respectively. Note that for the period since 1980, when *NAO* has been more important than what has been usual during the century, the latter's strongest lag (20% of ERR) is also 1 year. Finally, during the period in the second half of the century when *LSST* becomes particularly important, there is a mix of lags for *LSST* with significant signal, between 0 and 2 years, although a lag of 1 year has the longest period of contributing 20–25% of ERR. We will consider more fully the possible physical mechanisms underlying all these model characteristics in the Discussion section. Note also that the monthly analysis of Section 3.2 leads to a clearer, and physically realistic, view of the lag relationships.

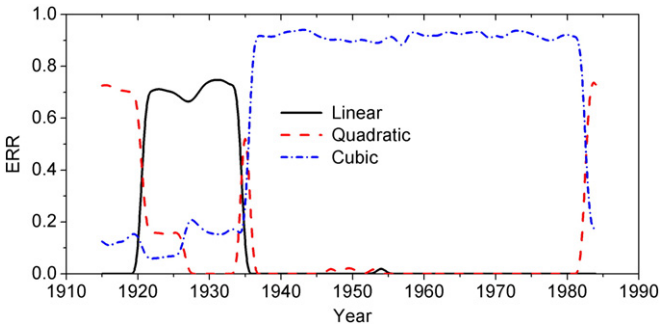

Fig. 5. A comparison of importance of the polynomial rank in terms over time considering four input variables based on annual data. To avoid inconsistencies in presentation due to initial and final conditions in the dataset, the initial (before 1915) and final (after 1984) ERR contributions were ignored due to insufficient samples.

3.1.3. Two input variables: SMB and NAO

In this case, only two input variables (*SMB* and *NAO*) were considered so the 30-year sliding window NFIR model can be written in an analogous way to Eq. (9), but without the *LSST* component. As expected from the earlier results, *SMB* is the dominant input variable from this pair over the whole century, explaining 40–70% of ERR (Fig. 6b). The model characteristics in terms of dominant polynomial degrees and lags are very similar for the dominant variable, *SMB* (Figs. S1–S2). This is less true for the lags for *NAO* (Fig. S3), but the magnitude of these terms is small. Note that the total ERR (Fig. 6b) is somewhat less than in the previous model (60–80%), consistent with this test explaining much of the signal, through *SMB*, but missing 10–20% of ERR (through the absence of *LSST*).

3.1.4. Two input variables: SMB and LSST

For this test, a different set of two variables (*SMB* and *LSST*) were considered as inputs for the NFIR model. Again as expected from the earlier results, *SMB* is the dominant input variable from this pair for much of the century, usually accounting for at least 50% of ERR (Fig. 6c). However, *LSST* always contributes more than 10% and is even the largest term, explaining 70% of the ERR, during the 1960s. This is similar to the case in the model containing all three input variables. The model characteristics in terms of dominant polynomial degrees and lags are very similar, but now for both variables (Figs. S4–S6). The ERR sum is similar (80–90%) to that of the model with all three input variables. *LSST*, while being less important in the model than *SMB*, is clearly a vital ingredient without which a model is quite different.

3.1.5. Two input variables: LSST and NAO

For this final model test of the annual data, the remaining two-variable combination (*LSST* and *NAO*) was considered. With the dominant input of *SMB* no longer included in the model, the structure of the model must change significantly. However, consistent with the last two tests, the dominant term now becomes *LSST*, with 50–70% of ERR explained except for a short time in the 1950s, and in recent decades, when *NAO* has attained a similar influence to *LSST* (Fig. 6d). Other elements of the model do indeed change. The dominant polynomial is now generally a quadratic (Fig. S7) and the temporal variability of the lags is somewhat different also (Figs. S8–S9), except in the 1960s–'80s, when all the sensitivity tests place *LSST* as the dominant term. During this interval, the mixed importance for *LSST* lags of 0–2 years found in the complete model (Fig. 8) emerges once more. The ERR sum is normally somewhat less than for the complete model, or the *SMB* with *LSST* case, but sometimes as high as these (70–90%). It is relevant here, and for the Discussion, that Bigg et al. (2014) found a strong correlation between *NAO* and the local *SMB* in the vicinity of calving glaciers.

3.2. Test 2: Monthly data analysis

Given that the peak month for iceberg numbers at 48°N is May (Bigg and Wilton, 2014; Marko et al., 1994), yet calving is most likely to occur during high summer (Howat et al., 2010), the lag between calving and I48N is likely to be the best part of a year, or annual multiples of such a period. In this test, therefore, the monthly input variable data from 1900–2008 were used to model the monthly I48N series to determine if more detail on the lags involved can be identified from monthly NFIR models than is possible from purely annual data. Using a 30-year sliding window again, there are now 360 samples of data for each window. This provides a better chance of producing a more accurate model comparing with only 30 samples of data for each window for the annual data analysis. However, for the monthly analysis, the required memory and computation time are dramatically increased because of the increase in the number of candidate terms. There are 148 possible candidate terms considering linear terms only, 11,026 possible candidate terms considering quadratic terms, and 551,300 possible candidate

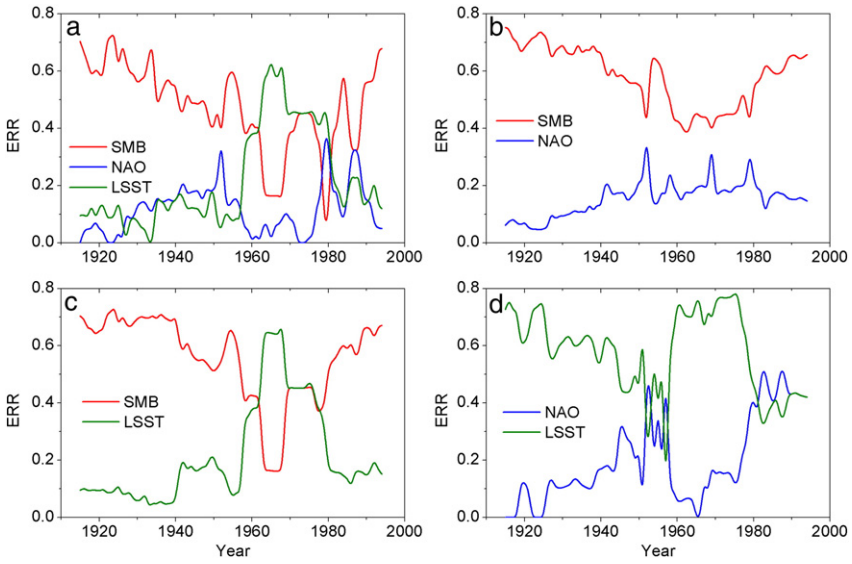

Fig. 6. Computed contributions of variables to I48N over time from 1900 to 2008, based on the ERR values for a 30-year sliding window which is incremented 1 year at a time, using annual time series. A) inputs: *SMB*, *NAO*, *LSST*; b) inputs: *SMB*, *NAO*; c) inputs: *SMB*, *LSST*; d) inputs: *NAO*, *LSST*. The following is true for all succeeding Figs. 7–11: to avoid inconsistencies in presentation due to initial and final conditions in the dataset, the initial (before 1915) and final (after 1994) ERR contributions were ignored due to insufficient samples.

terms considering cubic terms. To ease this computational burden, in the modelling of this section, only the linear and quadratic terms were considered. Inclusion of cubic terms has nevertheless been tested, but no significant improvement of model performance was achieved in comparison to a model without cubic terms.

3.2.1. Three input variables: SMB, NAO, and LSST

To begin the monthly analysis, all three input variables (*SMB*, *NAO*, and *LSST*) were considered for the NFIR model, which now can be written as:

$$\begin{aligned} I48N_m(k) = \; & f(SMB_m(k), SMB_m(k-1), \ldots, SMB_m(k-48), \\ & NAO_m(k), NAO_m(k-1), \ldots, NAO_m(k-48), \\ & LSST_m(k), LSST_m(k-1), \ldots, LSST_m(k-48)) \\ & +\varepsilon(k) \end{aligned} \tag{10}$$

where the maximum time lag was increased to 48 months to match the 4 years considered in the annual data analysis.

The temporal variability of the importance of the three inputs at monthly resolution (Fig. 9a) is similar to that of the annual model (Fig. 6a). *SMB*'s contribution to ERR is dominant for the first half of the record, with *LSST* being important during the 1960s–'80s. However, using monthly data, in contrast to the case for the annual model, *NAO* becomes the most important variable in recent years, contributing

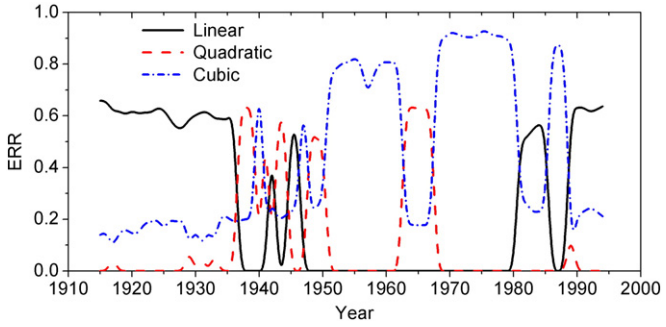

Fig. 7. A comparison of the importance of the different sort of polynomial terms by time considering three input variables (*SMB*, *NAO*, and *LSST*) for the model; based on annual data.

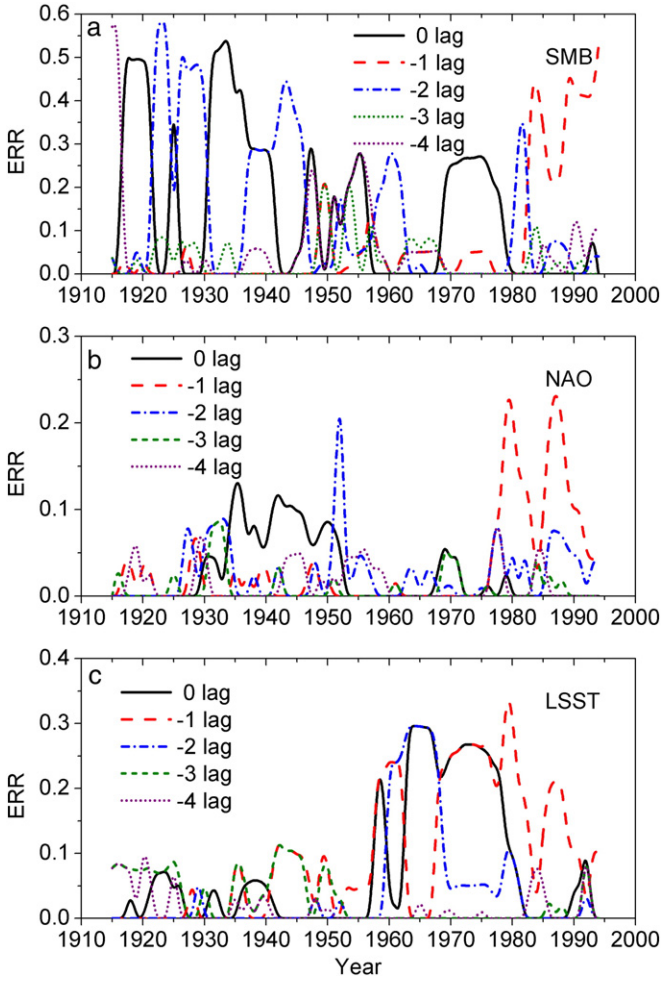

Fig. 8. Computed contributions to the annual I48N over 1900–2008 of the lags of a) *SMB*, b) *NAO*, and c) *LSST*. These lags are based on the ERR values for a 30-year sliding window, incremented 1 year at a time, where only one variable was considered as the input. Note the change in ERR scale between panels. After Fig. 6 of Bigg et al. (2013).

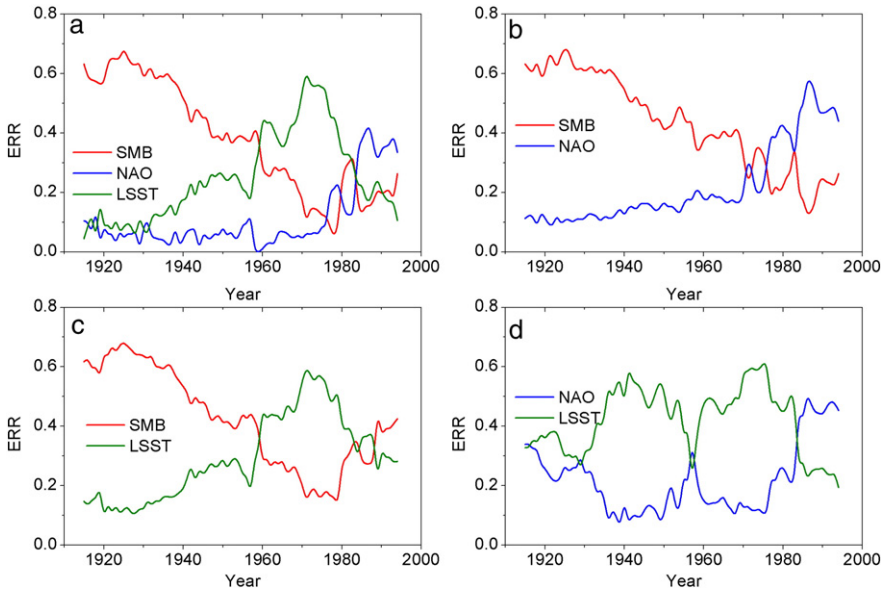

Fig. 9. Computed contributions of variables to I48N over time from 1900 to 2008, based on the ERR values for a 30-year sliding window which is incremented 1 year at a time, using monthly time series. a) inputs: *SMB*, *NAO*, *LSST*; b) inputs: *SMB*, *NAO*; c) inputs: *SMB*, *LSST*; d) inputs: *NAO*, *LSST*.

consistently ~40% to ERR over the last 15 years. With the greater variability inherent in monthly data, the total ERR, while good (~80%), tends to be a little less than the case for the annual model.

The sliding window's model complexity with monthly input data remains consistent over the whole study period, with quadratic terms contributing 60–70% of ERR throughout (Fig. 10). This is a distinct contrast to the modelling using the annual data (Fig. 7) where the degree of polynomial terms in the sliding window model varies significantly. When we turn to consider the important time lags in the model, it is clear that the most important time lags are not integral multiples of 12 (1 year), but vary depending on variable—18 months for *SMB*, 8/9 and 21/22 months for *LSST*, and 6 months for *NAO* (Fig. 11). We will consider this in more detail in the Discussion, but given the peak I48N in late spring/early summer, these lags imply that a range of environmental factors from the previous year, not the year of the iceberg arrival at 48°N, is likely to be the cause of the varying iceberg discharge from west Greenland.

3.2.2. Two input variables: SMB and NAO

In this case, only two input variables (*SMB* and *NAO*) were considered, and the 30-year sliding window NFIR model can be written in an analogous way to Eq. (10), but without the *LSST* component. As expected from the earlier results, *SMB* is the dominant input variable contributing to ERR from this pair over the first two thirds of the century

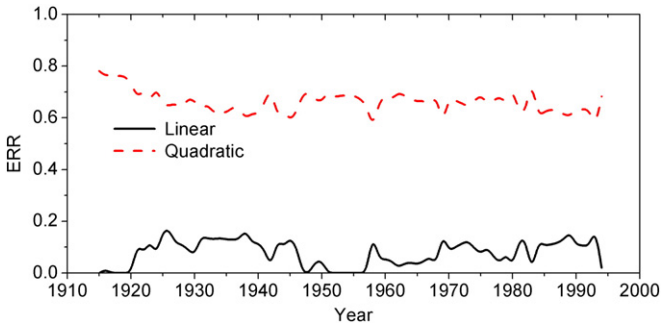

Fig. 10. A comparison of the importance of the polynomial rank in terms by time considering three input variables (*SMB*, *NAO*, and *LSST*) for the I48N model; based on monthly data.

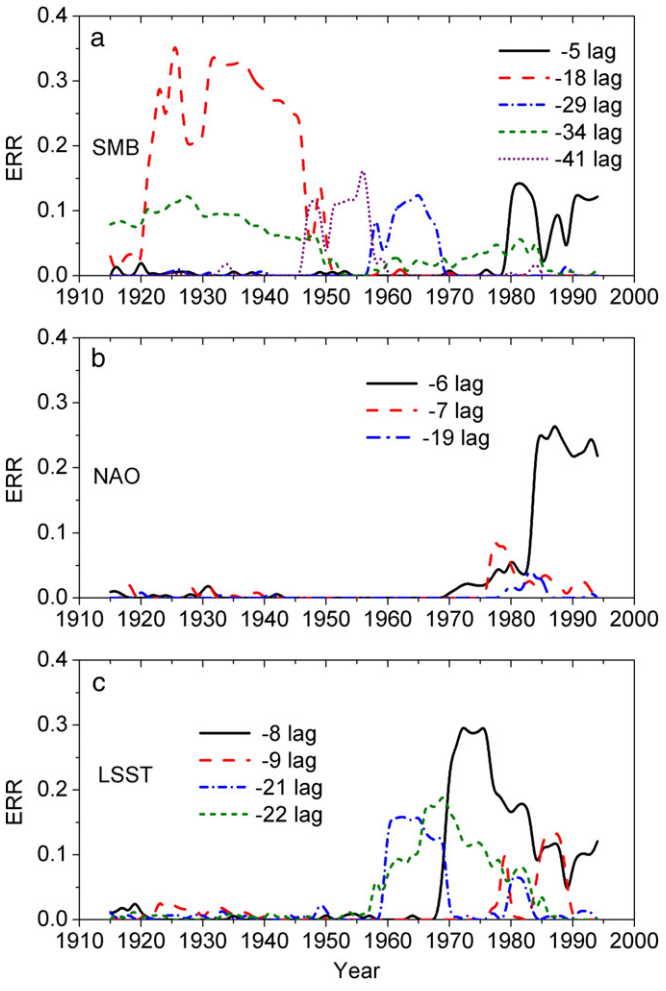

Fig. 11. Computed contributions to the monthly I48N over 1900–2008 of the lags of a) *SMB*, b) *NAO*, and c) *LSST*. These lags are based on the ERR values for a 30-year sliding window, incremented 1 year at a time, where only one variable was considered as the input.

(Fig. 9b), with *NAO* taking over dominance in the last few decades. The model characteristics in terms of dominant polynomial degrees and lags are very similar to the case for the 3 input variable monthly NFIR model at the times when either input variable in this case is dominant (Figs. S10–S12). Note that the total ERR (Fig. 9b) is somewhat less than in the previous model (~70%), consistent with this test explaining much of the signal, but missing a key element for several decades (*LSST*).

3.2.3. Two input variables: SMB and LSST

For this test, a different two variables (*SMB* and *LSST*) were considered as inputs for the NFIR model. Again as expected from the full model results, *SMB* is the dominant contributing variable to ERR from this pair for the first half of the century, with *LSST* taking over in importance for several decades thereafter (Fig. 9c). However, as the *NAO* is not represented, it is *SMB* that increases in importance in the last decade, although to a lesser extent than for the annual model. Once more the model characteristics in terms of dominant polynomial degrees and lags are very similar for both variables (Figs. S13–S15). The ERR sum is similar (~80%) to that of the model with all three input variables, except towards the end of the period, when it is less.

3.2.4. Two input variables: LSST and NAO

For this final model test of the monthly data, the remaining two-variable combination (*LSST* and *NAO*) was considered. With the dominant input of *SMB* not included in the model, the structure of the model changes (Fig. 9d), as was found for the annual model test. For much of the century, the dominant term contributing ~50% to ERR now becomes *LSST*, except for a few years in the 1950s, and in recent decades, when *NAO*'s contribution to ERR reaches this level. While the dominant polynomial in the model remains quadratic (Fig. S16) and the temporal variability of the lags for *NAO* is similar to that in the above monthly models containing this input variable (Fig. S17), the lag behaviour is somewhat different for *LSST* (Fig. S18). The important lags are the same, but 8 months is now more important over longer time periods than before (Fig. S17). Note that without the important *SMB* factor, the ERR sum is normally somewhat less than for the complete model at ~70%.

4. Discussion

A series of sensitivity studies has been carried out using the sliding window NFIR modelling approach to represent the I48N time series, a proxy for western Greenland iceberg flux. Despite the likely uncertainty over the time series during early decades, and the likelihood that not all factors contributing to I48N are fully encapsulated within the variation of our three chosen variables, we have found a notable consistency between these studies, whether using annual or monthly data, with the models explaining 80–90% of the variance in the I48N signal (Figs. 12 and 13).

We have used geographically large-scale factors as the input variables within our models and can therefore not hope to attribute detailed physical mechanisms at the glacier scale as the cause of the significant

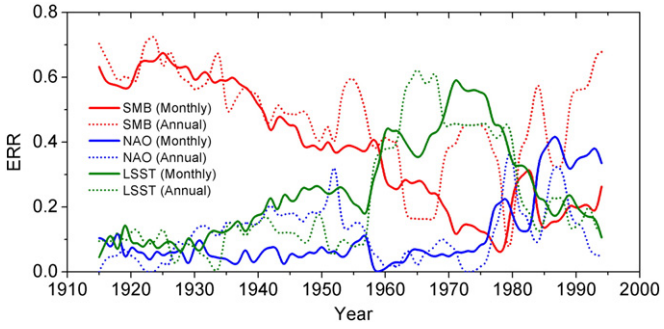

Fig. 13. A comparison of computed contributions of the three input variables of *SMB*, *LSST*, and *NAO* for full NFIR models based on monthly and annual data respectively.

variations in the model over time. However, in terms of explaining the ERR results for the range of the NFIR models of I48N, the GrIS *SMB* was a major factor contributing to the variability through much of the twentieth century and was particularly important in its first half. The *LSST* variable tends to be the second most important variable contributing towards the models' ERR, particularly dominating the models during the 1960s–'80s. Finally, the *NAO* variable, so often seen as a key factor underlying North Atlantic environmental change, is seen to be a generally minor contributor to explaining the variance of the I48N signal, except in the monthly model after the late 1980s (Fig. 9a).

The polynomial form of the NFIR model changes between being dominantly cubic for the annual model (Fig. 7) to dominantly quadratic for the monthly model (Fig. 10). This is partly dictated by the highest degree terms that could be included in the respective models but does highlight how, particularly in the monthly model where the strong seasonal cycle of I48N (Marko et al., 1994) needs to be reproduced, the model input–output relationships are non-linear for most models. Similarly, there are clear lags in the system, with compatible results in both annual (Fig. 8) and monthly models (Fig. 11). Thus, considering the more temporally resolving monthly models, when the *SMB* is the dominant variable for explaining the variance of the model in the first half of the century, there is a strong 18-month lead of this variable with respect to I48N. In contrast, during the period of the 1960s–'80s when *LSST* explained most variance, there is an 8/9 and 21/22-month input lead, while after 1985, towards the end of the series, when for the monthly model the *NAO* explained most variance, there is a notable 6/7-month lag (Fig. 11).

NARMAX models (and so the NFIR model used here) are not conventional process models, overtly linking input to output through physical equations. Neither are they simple statistical models, strongly guided by preconceptions of the user. They allow the user to seek understanding of the most statistically significant model to explain the output, given the limitations of the set of input variables, with a much freer complexity than is possible in conventional statistical approaches (Billings, 2013). Typically, the resulting model is non-linear, comprises of a number of terms, and, as in our study, allows the interaction between the inputs to readily change with time. As discussed in the

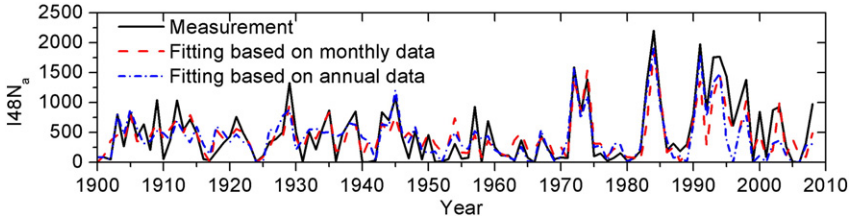

Fig. 12. A comparison of two model outputs (I48N) of NFIR models based on monthly and annual data, respectively. Three input variables (*SMB*, *NAO*, and *LSST*) were considered. The black solid curve depicts the observed annual total I48N; the red dash curve depicts the model output based on the monthly data, and the blue dash-dot curve depicts the model output based on the annual data.

Introduction, we chose three large-scale physical variables as inputs to match in principle, if not in the reality of detailed processes, the three mechanisms described by Straneo et al. (2013) as being responsible for glacier retreat. We now expand on this by returning to the basic physical mechanisms.

For much of the twentieth century, and most strongly in its first half, I48N's NFIR monthly models are dominated by the *SMB* terms, in a non-linear way (Fig. 10). There is a divergence between annual and monthly models in this non-linearity in the less well-observed times before 1930, although the latter is still strongly quadratic in form during this period. The coefficient of the leading model term involving *SMB* is negative for the majority of sliding window models, and the *SMB* lag term explaining more of the ERR is 18 months during the first half the twentieth century (Fig. 11). A lower *SMB* typically occurs because the runoff is high (Hanna et al., 2011). Our hypothesis here is that additional runoff towards the end of a summer season may lead to more calving next year, and thus a higher I48N flux the following spring. The physical mechanisms by which this could occur are through increased crevassing and bed lubrication (Andersen et al., 2011; Moon et al., 2014). It is also known that increased runoff enhances plume formation, fjord water entrainment, and so submarine melting at the glacier terminus (Sciascia et al., 2013). Additional runoff towards the end of summer may also lead to extra undercutting of the calving front, effectively priming it for rapid breakup the following year following removal of the melange (Slater et al., 2015). Thus, while the results of the NFIR modelling cannot directly imply causality, there are physical routes by which changes in *SMB*, and hence the model, could lead to changes in I48N.

From around 1990, there is a divergence between annual and monthly models, with the *NAO*'s contribution to the model variance becoming more important in the latter. It is noteworthy that this date is also when *SMB* began falling rapidly (Hanna et al., 2011; Rignot et al., 2011) as Greenland warmed (Hanna et al., 2013). The most important lag terms for both the *SMB* and *NAO* contributions to the monthly model variance also switch to 5–6 months at this time. This change in dominant model lag is consistent with the melting to calving link being shortened in recent years to the same season. Thus, since the early 1990s, both the decreasing *NAO* and *SMB* (Fig. 1) have led to increased runoff locally, and, we postulate, resulting in calving the same season (O'Leary and Christoffersen, 2013; Sole et al., 2011), and so a peak in I48N the following spring.

The other contributing variable to the NFIR model is *LSST*, whose contribution to explaining the I48N variance is important throughout the second half of the twentieth century, but dominant between the late 1950s and early 1980s (Fig. 9a). Again there cannot be a directly attributable link between the model's *LSST* behaviour and calving. Indeed, changes in *LSST* will only be linked to changes in mechanisms such as submarine-ice melting during periods of strong winter convection in the Labrador Sea (such as the 1960s and '70s (Dickson et al., 1996)). However, *LSST* may be important in determining the extent, thickness, and duration of the ice melange in the fjord in front of the ice front (Walter et al., 2012). Interestingly, as with *SMB*, the most important lag terms involving *LSST*, and so contributing towards explaining the model variance, switch, from ~21 to 22 months to 8 to 9 in the last few decades. The increasing *LSST* and decreasing *SMB* of recent years (Fig. 1) are both potentially linked to increased runoff and calving so both these lag changes suggest a possible quickening of the response of calving to environmental change recently. In addition, while Jakobshavn Isbrae's contribution to I48N will only be a partial reason for its change (Wilton et al., 2015), the dramatic change in calving properties initiated from the late 1990s (Csatho et al., 2008) may also have contributed to this quickening pace of change.

5. Conclusion

Using a control engineering approach to data analysis that has not been used for environmental data before, we have shown that NIFR modelling provides strong statistical relationships between a plausible set of large-scale physical variables and I48N, a proxy for western Greenland iceberg flux. The NIFR model also suggests that the model best explaining the I48N variance has changed markedly, both in dominant variable and dominant lags, over the last century. These relationships are shown to generally be non-linear (Fig. 10) and not simply linked to a single process. Nevertheless, the modelling results are consistent with the underlying cause of calving during periods of change being related to surface runoff, and consequent changes in englacial and subglacial (Andersen et al., 2011) hydrology and submarine melting (Sciascia et al., 2013). Our NFIR modelling suggests that ice melange melting, leading to glacier calving front destabilisation, by the ocean may also frequently be important, but possibly more typically so in periods when other processes are stable (see Fig. 1). During the last few decades, however, the model is consistent with the mix of likely causes of calving becoming more complex, with the NIFR model suggesting that all processes are playing a non-negligible role, but there also being a shortening of the response time of Greenland glacial systems to environmental change. This may have led to the more interannually variable I48N of the 2000s, but it should be noted that 2 of the top 10 annual figures for the 1900–2014 time series of I48N have occurred since 2008. Given likely continued increases in ocean temperature and GrIS runoff, enhanced iceberg flux is predicted to continue in the years to come.

Acknowledgements

Funding was provided by the Natural Environmental Research Council (NERC) grant NE/H023402/1, EPSRC Platform grant EP/H00453X/1, and European Research Council Advanced Investigator Grant NSYS 226037. We would like to thank P. Huybrechts for supplying the runoff model used to calculate the *SMB* used here. The Kaplan v2 SST is available from NOAA's Physical Sciences Division (http://www.esrl.noaa.gov/psd). The *NAO* time series is available from the Climate Analysis Section, NCAR, Boulder, USA (http://climatedataguide.ucar.edu/category/data-set-variables/climate-indices/nao). The NEW series is available from the Institute for Ocean Technology (http://www.icedata.ca/Pages/NL_IceExtent/NL_index.php).

Appendix A

A.1. Adaptive–forward–OLS

The orthogonal least squares (OLS) algorithm (Billings, 2013; Leontaritis and Billings, 1985b) is a popular approach that has been widely used in non-linear system identification where the orthogonal least squares searches through all the possible candidate model terms to select the most significant model terms which are then included to build models term by term. The significance of each of the selected model terms is measured by an index, called the error reduction ratio (ERR), which indicates how much of the variance change in the system response, in percentage terms, can be accounted for by including the relevant model terms. Complex non-linear dynamic models and non-linear noise models can all be identified using this algorithm.

Consider a function in linear-in-the-parameters form

$$y(k) = \sum_{i=1}^{N} \theta_i p_i(k), k = 1, \ldots, M \tag{A1}$$

where $y(k)$ is the dependent variable or the term to regress upon, $p_i(k)$ are regressors, θ_i are unknown parameters to be estimated, M denotes the number of data points in the dataset, and N denotes the, as yet undetermined, number of terms in the model. Equation (A1) can be written as $Y = P\Theta$ where

$$Y = \begin{bmatrix} y(1) \\ \vdots \\ y(M) \end{bmatrix}, P = \begin{bmatrix} P^T(1) \\ \vdots \\ P^T(M) \end{bmatrix}, \Theta = \begin{bmatrix} \theta(1) \\ \vdots \\ \theta(N) \end{bmatrix} \tag{A2}$$

and $P^T(k) = (p_1(k),..., p_N(k))$. Matrix P can be decomposed as $P = W \times A$ where

$$W = \begin{bmatrix} w_1(1) & \dots & w_N(1) \\ \vdots & \vdots & \vdots \\ w_1(M) & \dots & w_N(M) \end{bmatrix} \tag{A3}$$

is an orthogonal matrix because

$$W^T W = Diag\left[\sum_{t=1}^{M} w_1^2(k), \dots, \sum_{t=1}^{M} w_N^2(k)\right] \tag{A4}$$

and A is an upper triangular matrix with unity diagonal elements

$$A = \begin{bmatrix} 1 & a_{12} & a_{13} & \cdots & a_{1N} \\ & 1 & a_{23} & \cdots & a_{2N} \\ & & \ddots & \ddots & \vdots \\ & & & 1 & a_{N-1N} \\ & & & & 1 \end{bmatrix} \tag{A5}$$

Therefore, $Y = P\Theta$ can be rewritten as $Y = WG$, where $G = A\Theta = [g_1,..., g_N]^T$. The estimation of the original parameters can be computed from

$$\left.\begin{aligned} \hat{\theta}_N &= \hat{g}_N \\ \hat{\theta}_i &= \hat{g}_i - \sum_{j=i+1}^{N} a_{ij}\hat{\theta}_j, i = N-1, \dots, 1 \end{aligned}\right\} \tag{A6}$$

To stop the search procedure and determine N, the number of significant terms, a criteria called penalised error-to-signal ratio (PESR), written as

$$PESR_n = \frac{1}{(1-\lambda n/M)^2}\left(1 - \sum_{i=1}^{n}[err]_i\right) \tag{A7}$$

was introduced to monitor the regressor search procedure, where n denotes the number of selected terms and $[err]_i$ is the error reduction ratio for each term. The search procedure stops when $[PESR]_n$ arrives at a minimum. The effect of the adjustable parameter λ on the results is discussed in Billings and Wei (2008).

The whole procedure can be summarised as follows:

1. Set $a_{11} = 1$, $w_1(k) = p_1(k)$, and $\hat{g}_1 = \frac{\sum_{k=1}^{M} w_1(k)y(k)}{\sum_{k=1}^{M} w_1^2(k)}$.
2. Set $a_{jj} = 1$and then calculate $a_{ij} = \frac{\sum_{k=1}^{M} w_i(k)p_j(k)}{\sum_{k=1}^{M} w_i^2(k)}$ for $j = 2,..., N$, where $i = 1,..., j-1$. Next, calculate $w_j(k) = p_j(k) - \sum_{i=1}^{j-1} a_{ij} w_i(k)$, and $\hat{g}_j = \frac{\sum_{k=1}^{M} w_j(k)y(k)}{\sum_{k=1}^{M} w_j^2(k)}$. Then calculate the ERR value, defined as

$$[err]_j = \frac{\hat{g}_j^2 \sum_{k=1}^{M} w_j^2(k)}{\sum_{j=1}^{M} y^2(k)} \tag{A8}$$

3. Compute the value of $PESR_j$ using (A7). The search procedure stops when $PESR_j$ arrives at a minimum. Ideally, the trend of $PESR_j$ takes the shape of a valley if values of $PESR_j$ for all candidate terms are calculated. The search procedure stops when $PESR_j$ arrives at the valley. Practically, it stops at the point before $PESR_j$ starts to rise. If there is no minimum at all, the search will continue until all candidate terms are scanned.

Appendix B. Supplementary data

Supplementary data to this article can be found online at http://dx.doi.org/10.1016/j.coldregions.2015.08.006.

References

Andersen, M.L., Nettles, M., Elosegui, P., Larsen, T.B., Hamilton, G.S., Stearns, L.A., 2011. Quantitative estimates of velocity sensitivity to surface melt variations at a large Greenland outlet glacier. J. Glaciol. 57, 609–620.

Berkson, J.M., Allen, A.A., Murphy, D.L., Boda, K.J., 2010. Integrated Ocean Observing System (IOOS (R)) supports marine operations: a look from the US Coast Guard. Mar. Technol. Soc. J. 44, 156–165.

Bigg, G.R., 1999. An estimate of the flux of iceberg calving from Greenland. Arct. Antarct. Alp. Res. 31, 174–178.

Bigg, G.R., Wilton, D.J., 2014. The iceberg risk in the Titanic year of 1912: was it exceptional? Weather 69, 100–104.

Bigg, G.R., Wei, H., Wilton, D.J., Zhao, Y., Billings, S.A., Hanna, E., Kadirkamanathan, V., 2014. A century of variation in the dependence of Greenland iceberg calving on ice sheet surface mass balance and regional climate change. Proc. R. Soc. Ser. A 470, 20130662.

Billings, S.A., 2013. Non-linear System Identification: NARMAX, Methods in the Time, Frequency, and Spatio-Temporal Domains. Wiley, London.

Billings, S.A., Wei, H., 2007. Sparse model identification using a forward orthogonal regression algorithm aided by mutual information. IEEE Trans. Neural Netw. 81, 306–310.

Billings, S.A., Wei, H., 2008. An adaptive orthogonal search algorithm for model subset selection and nonlinear system identification. Int. J. Control. 81, 714–724.

Box, J.E., 2013. Greenland ice sheet surface mass balance reconstruction. Part II: surface mass balance. J. Clim. 26, 6974–6989.

Chen, S., Billings, S.A., 1989. Representation of non-linear systems: the NARMAX model. Int. J. Control. 49, 1013–1032.

Chen, S., Billings, S.A., Luo, W., 1989. Orthogonal least squares methods and their application to nonlinear system identification. Int. J. Control. 50, 1873–1896.

Christensen, E., Luzader, J., 2012. From sea to air to space, a century of iceberg tracking technology. Coast Guard Proc. Mar. Saf. Sec. Counc. 69, 17–22.

Csatho, B., Schenk, T., van der Veen, C.J., Krabill, W.B., 2008. Intermittent thinning of Jakobshavn Isbrae, West Greenland, since the Little Ice Age. J. Glaciol. 54, 131–144.

Dickson, R., Lazier, J., Meincke, J., Rhines, P., Swift, J., 1996. Long-term coordinated changes in the convective activity of the North Atlantic. Prog. Oceanogr. 38, 241–295.

Enderlin, E.M., Howat, I.M., Jeong, S., Noh, M.J., van Angelen, J.H., van den Broeke, M.R., 2014. An improved mass budget for the Greenland ice sheet. Geophys. Res. Lett. 41, 866–872.

Fettweis, X., Hanna, E., Gallée, H., Huybrechts, P., Erpicum, M., 2008. Estimation of the Greenland ice sheet surface mass balance during twentieth and twenty-first centuries. Cryosphere 2, 117–129.

Hanna, E., Huybrechts, P., Cappelen, J., Steffen, K., Bales, R.C., Burgess, E., McConnell, J., Steffensen, J.P., Van den Broeke, M., Wake, L., Bigg, G.R., Griffiths, M., Savas, D., 2011. Greenland Ice Sheet surface mass balance 1870 to 2010 based on Twentieth Century Reanalysis, and links with global climate forcing. J. Geophys. Res. - Atmos. 116, D24121.

Hanna, E., Jones, J.M., Cappelen, J., Mernild, S.H., Wood, L., Stekken, K., Huybrechts, P., 2013. The influence of North Atlantic atmosdpheric and oceanic forcing effects on 1900-2012 Greenland summer climate and ice melt/runoff. Int. J. Climatol. 33, 862–880.

Hill, B.T., Jones, S.J., 1990. The Newfoundland ice extent and the solar cycle from 1860 to 1988. J. Geophys. Res. 95, 5385–5394.

Howat, I.M., Box, J.E., Ahn, Y., Herrington, A., McFadden, E.M., 2010. Seasonal variability in the dynamics of marine-terminating outlet glaciers in Greenland. J. Glaciol. 56, 601–613.

Hurrell, J.W., Deser, C., 2009. North Atlantic climate variability: the role of the North Atlantic Oscillation. J. Mar. Syst. 78, 28–41.

Janssens, I., Huybrechts, P., 2000. The treatment of meltwater retention in mass-balance parameterisations of the Greenland ice sheet. Ann. Glaciol. 31, 133–140.

Kaplan, A., Cane, M., Kushnir, Y., Clement, A., Blumenthal, M., Rajagopalan, B., 1998. Analyses of global sea surface temperature 1856–1991. J. Geophys. Res. Oceans 103, 18567–18589.

Kjaer, K.H., Khan, S.A., Korsgaard, N.J., Wahr, J., Bamber, J.L., Hurkmans, R., van den Broeke, M., Timm, L.H., Kjeldsen, K.K., Bjork, A.A., Larsen, N.K., Jorgensen, L.T., Faerch-Jensen, A., Willersley, E., 2012. Aerial photographs reveal late-20th-century dynamic ice loss in Northwestern Greenland. Science 337, 569–573.

Leontaritis, I.J., Billings, S.A., 1985a. Input-output parametric models for non-linear systems. Part I: deterministic non-linear systems. Int. J. Control. 41, 303–328.

Leontaritis, I.J., Billings, S.A., 1985b. Input-output parametric models for non-linear systems. Part II: stochastic non-linear systems. Int. J. Control. 41, 329–344.

Marko, J.R., Fissel, D.B., Wadhams, P., Kelly, P.M., Brown, R.D., 1994. Iceberg severity off eastern North America: its relationship to sea ice variability and climatic change. J. Clim. 7, 1335–1351.

Moon, T., Joughin, I., Smith, B., van den Broeke, M.R., van den Berg, W.J., Noel, B., Usher, M., 2014. Distinct patterns of seasonal Greenland glacier velocity. Geophys. Res. Lett. 41, 7209–7216.

Motyka, R.J., Dryer, W.P., Amundson, J., Truffer, M., Fahnstock, M., 2013. Rapid submarine melting driven by subglacial discharge, LeConte Glacier, Alaska. Geophys. Res. Lett. 40. http://dx.doi.org/10.1002/grl.51011.

Mugford, R.I., Dowdeswell, J.A., 2010. Modeling iceberg-rafted sedimentation in high-latitude fjord environments. J. Geophys. Res. 115, F03024.
Murphy, D.L., Cass, J.L., 2012. The International Ice Patrol: safeguarding life and property at sea. Coast Guard Proc. Mar. Saf. Sec. Counc. 69, 13–16.
O'Leary, M., Christoffersen, P., 2013. Calving on tidewater glaciers amplified by submarine frontal melting. Cryosphere 7, 119–128.
Reeh, N., 1994. Calving from Greenland glaciers: observations, balance estimates of calving rates, calving laws. Workshop on the calving rate of West Greenland glaciers in response to climate change. Danish Polar Centre, Copenhagen (171 pp.).
Rignot, E., Box, J.E., Burgess, E., Hanna, E., 2008. Mass balance of the Greenland ice Sheet from 1958 to 2007. Geophys. Res. Lett. 35, L20502.
Rignot, E., Velicogna, I., van den Broecke, M.R., Monaghan, A., Lenaerts, J.T.M., 2011. Acceleration of the contribution of the Greenland and Antarctic ice sheets to sea level rise. Geophys. Res. Lett. 38, L05503.
Sasgen, I., van den Broeke, M., Bamber, J.L., Rignot, E., Sorensen, L.S., Wouters, B., Martinec, Z., Velicogna, I., Simonsen, S.B., 2012. Timing and origin of recent regional ice-mass in Greenland. Earth Planet. Sci. Lett. 333, 293–303.
Sciascia, R., Straneo, F., Cenedese, C., Heimbach, P., 2013. Seasonal variability of submarine melt rate and circulation in an East Greenland fjord. J. Geophys. Res. Oceans 118. http://dx.doi.org/10.1002/jgrc.20142.
Seale, A., Chrisoffersen, P., Mugford, R.I., O'Leary, M., 2011. Ocean forcing of the Greenland Ice Sheet, calving fronts and patterns of retreat identified by automatic satellite monitoring of eastern outlet glaciers. J. Geophys. Res. 116, F03013.
Slater, D.A., Nienow, P.W., Cowton, T.R., Goldberg, D.N., Sole, A.J., 2015. Effect of near-terminus subglacial hydrology on tidewater glacier submarine melt rates. Geophys. Res. Lett. 42, 2861–2868.
Sohn, H.G., Jezek, K.C., van der Veen, C.J., 1998. Jakobshavn Glacier, West Greenland: 30 years of spaceborne observations. Geophys. Res. Lett. 25, 2699–2702.
Sole, A.J., Mair, D.W.F., Nienow, P.W., Batholomew, I.D., King, M.A., Burke, M.J., Joughin, I., 2011. Seasonal speedup of a Greenland marine-terminating outlet glacier forced by surface-melt induced changes in subglacial hydrology. J. Geophys. Res. Earth Surf. 116, F03014.
Straneo, F., Heimbach, P., Sergienko, O., Hamilton, G., Catania, G., Griffies, S., Hallberg, R., Jenkins, A., Joughin, I., Motyka, R., Pfeffer, W.T., Price, S.F., Rignot, E., Scambos, T., Truffer, M., Vieli, A., 2013. Challenges to understanding the dynamic response of Greenland's marine terminating glaciers to oceanic and atmospheric forcing. Bull. Am. Meteorol. Soc. 94, 1131–1144.
Todd, J., Christoffersen, P., 2014. Are seasonal calving dynamics forced by buttressing from ice melange or undercutting by melting? Outcomes from full-Stokes simulations of Store Glacier, West Greenland. Cryosphere 8, 2353–2365.
Van den Broeke, M., Bamber, J., Ettema, J., Rignot, E., Schrama, E., van den Berg, W.J., van Meijgaard, E., Velicogna, I., Wouters, B., 2009. Partitioning recent Greenland mass loss. Science 326, 984–986.
Walter, J.I., Box, J.E., Tulaczyk, S., Brodsky, E.E., Howat, I.M., Ahn, Y., Brown, A., 2012. Oceanic mechanical forcing of a marine-terminating Greenland glacier. Ann. Glaciol. 53, 181–192.
Wei, H.L., Billings, S.A., Liu, J., 2004. Term and variable selection for nonlinear system identification. Int. J. Control. 77, 86–110.
Wei, H.L., Billings, S.A., Zhao, Y., Guo, L.Z., 2009. Lattice dynamical wavelet neural networks implemented using particle swarm optimization for spatio-temporal system identification. IEEE Trans. Neural Netw. 20, 181–185.
Wilton, D.J., Bigg, G.R., Hanna, E., 2015. A coupled ocean-iceberg model forced with data from the Twentieth Century Reanalysis project: global circulation, modelling iceberg flux at 48°N and implications for west Greenland iceberg discharge 1900-2008. Prog. Oceanogr. http://dx.doi.org/10.1016/j.pocean.2015.07.003 (in press).
Zhao, Y., Billings, S.A., Wei, H.L., Sarrigannis, P.G., 2012. Tracking time varying causality and directionality of information flow using an error reduction test with applications to electroencephalography data. Phys. Rev. E 86, 051919.
Zou, R., Chon, K.H., 2004. A robust algorithm for estimation of time-varying transfer functions. IEEE Trans. Biomed. Eng. 51, 219–228.
Zou, R., Wang, H., Chon, K.H., 2003. A Robust time-varying identification, algorithm using basis functions. Ann. Biomed. Eng. 31, 840–853.